

Zhao Q, Wang C, Guo J, Wang B, Liu J.

[Precise orbit and clock determination for BeiDou-3 experimental satellites
with yaw attitude analysis.](#)

GPS Solutions 2018, 22, 4.

Copyright:

The final publication is available at Springer via <https://doi.org/10.1007/s10291-017-0673-y>

DOI link to article:

<https://doi.org/10.1007/s10291-017-0673-y>

Date deposited:

24/01/2018

Embargo release date:

04 November 2018



This work is licensed under a [Creative Commons Attribution-NonCommercial 3.0 Unported License](#)

25 on the sun elongation angle were identified in SLR residuals for the BeiDou-3e IGSO C32
26 satellite, while such errors did not exist for BeiDou-2 IGSO/MEO and BeiDou-3e MEO
27 satellites. No orbit accuracy degeneration for BeiDou-3e IGSO and MEO satellites was
28 observed when the elevation angle (β angle) of the sun above the orbital plane was between
29 -4° and $+4^\circ$. In that case, the BeiDou-2 IGSO and MEO satellites are in orbit normal (ON)
30 mode. An analysis of the yaw attitude identified that BeiDou-3e satellites did not use the ON
31 mode, but experienced midnight- and noon-point maneuvers when the β angle is
32 approximately between -3° and $+3^\circ$. Compared with BeiDou-2 satellites, the onboard clocks
33 of the BeiDou-3e IGSO satellites showed dramatic improved performance. The stability of
34 BeiDou-3e IGSO satellites can be compared to the latest type of RAFSs employed onboard
35 the GPS IIF satellites as well as the PHMs used onboard the Galileo satellites.

36 **Keywords:** BeiDou-3; precise orbit determination; clock analysis; passive hydrogen
37 masers; yaw attitude

38

39 **Introduction**

40 The development of the Chinese BeiDou Navigation Satellite System (BDS) occurs in 3 phases.
41 In the first phase, BeiDou-1, 4 satellites were deployed to geostationary orbit (GEO) to form an
42 experimental system. The second phase, BeiDou-2, launched a constellation of 5 satellites in GEO,
43 5 in inclined geosynchronous orbit (IGSO), and 4 in medium earth orbit (MEO). In this phase, the
44 system has been providing continuous passive positioning, navigation, and timing (PNT) services
45 for users throughout the Asia-Pacific area since December 27, 2012. In the third phase (BeiDou-
46 3), the BDS will be completed with global navigation ability by 2020. At that time, the system will
47 comprise a constellation of 5 GEO, 27 MEO, and 3 IGSO satellites (CSNO 2016). On March 30,
48 2015, the first BeiDou-3 satellite was successfully launched into IGSO, beginning the system's
49 transition toward global coverage. Up to May 2017, there were 5 BeiDou-3 satellites in orbit, as
50 listed in Table 1. Currently, 4 satellites (C31–C34) are already in operation and broadcasting

51 signals, while C35 is still being tested. The purpose of the 5 satellites is to validate the new features
 52 of the BeiDou-3 satellites, including signals, intersatellite link technology, and onboard frequency
 53 standards. Hence, these 5 satellites are referred as BeiDou-3 experimental satellites, hereafter
 54 abbreviated as BeiDou-3e.

55

56 **Table 1** Status of BeiDou-3e satellites (May 2017). CAS: China Academy of Science; CAST:
 57 China Academy of Space Technology

Satellite	Launch date	COSPAR ID	PRN	Orbit	Manufacturer
I1-S	Mar. 30, 2015	2015-019 A	C31	IGSO, 55° inclination	CAS
M1-S	Jul. 25, 2015	2015-037 A	C34	MEO	CAST
M2-S	Jul. 25, 2015	2015-037 B	C33	MEO	CAST
I2-S	Sep. 29, 2015	2015-053 A	C32	IGSO, 55° inclination	CAST
M3-S	Feb. 1, 2016	2016-006 A	C35	MEO	CAS

58

59 All BeiDou-2 satellites are based on the DongFangHong-3A (DFH-3A) satellite platform, which
 60 is an updated version of DFH-3 used by BeiDou-1 satellites and manufactured by the China
 61 Academy of Space Technology (CAST). The DFH-3A bus adopts a hexahedral structure, and
 62 additional equipment for C-band telecommunication and short message service have been carried
 63 by GEO satellites. The BeiDou-2 satellites also support 2-way satellite time and frequency transfer
 64 to enable the determination of satellite clock offsets.

65 However, BeiDou-3e satellites are based on two different satellite platforms developed by
 66 CAST and the China Academy of Science (CAS). The CAS platform weighs only approximately

67 848 kg. Similar to Galileo-IOV/FOC satellites, it has an elongated shape along X axis instead of a
68 cubic one, and the elongated face with the normal direction along Z axis points to the earth's center.
69 In addition, a star camera instead of sun and earth sensors is used to determine attitude and stabilize
70 the satellite's orientation. On the other hand, the CAST platform has a cubic shape and weighs
71 2800 kg. Other improved technologies have also been used for both platforms. For example, the
72 intersatellite link manages communication and distance measurement between the BeiDou-3e
73 satellites to enable autonomous navigation, and improves independency and stability of BDS. With
74 intersatellite ranging measurements, precise orbits can be determined (Yang et al. 2017). The
75 primary frequency standards of the BeiDou-2 navigation payload are based on Chinese rubidium
76 clocks, while European clocks serve as backup units. However, passive hydrogen masers (PHMs)
77 developed by Shanghai Astronomical Observatory and Beijing Institute of Radio Metrology and
78 Measurement have been used to provide the primary frequency standard for BeiDou-3 satellites.
79 The improved Chinese rubidium atomic frequency standards (RAFSs) serve as the backup.

80 Precise orbits and clocks are key requirements for the most demanding applications of the
81 BDS. Much research has been done on the precise orbit determination (POD) of BeiDou-2
82 satellites (Zhao et al. 2013; Steigenberger et al. 2013; Lou et al. 2014). In general, the 3D RMS of
83 orbit differences for the orbit products from the International GNSS Service (IGS) Multi-GNSS
84 Experiment (MGEX) analysis centers (ACs) is 12 to 26 cm for MEOs, 32 to 51 cm for IGSOs, and
85 approximately 510 cm for GEOs (Montenbruck et al. 2017). In addition, satellite laser ranging
86 (SLR) validation demonstrates that the radial orbit accuracy for MEO, IGSO, and GEO satellites
87 is approximately 5 cm, 10 cm, and 50 cm respectively (Montenbruck et al. 2017). However,
88 BeiDou-2 satellites suffer solar radiation pressure (SRP) model deficiency, which is mainly caused
89 by the attitude control mode. For BeiDou-2 IGSO and MEO satellites, 2 kinds of attitude modes
90 are used: yaw steering (YS) and orbit normal (ON). Dramatic orbit accuracy degeneration can be
91 observed when satellites switch the attitude mode or are in the ON mode. Based on the proper yaw
92 attitude model for BeiDou-2 IGSO and MEO satellites (Feng et al. 2014; Guo et al. 2017a), some
93 efforts have been done to construct a better SRP model for BeiDou-2 IGSO and MEO satellites in

94 the ON mode (Guo 2014; Guo et al. 2017a; Prange et al. 2016). In addition, Guo et al. (2017a)
95 identified a deficiency in the 5-parameter empirical Extended CODE Orbit Model (ECOM) SRP
96 model (Beutler et al. 1994, Springer et al. 1999) in YS mode for BeiDou-2 IGSO satellites, and
97 proposed that the deficiency can be overcome by using the box-wing model as the a priori SRP
98 model. For BeiDou-2 GEO satellites, because the ON mode is used as well as almost static
99 observation conditions with respect to ground stations, the orbit accuracy is at the meter level.

100 Limited research has been done on orbit and clock determination for BeiDou-3e satellites,
101 except for Tan et al. (2016). In that work, precise orbits were determined based on 1-month data
102 from 9 International GNSS Monitoring and Assessment System (iGMAS) tracking stations. The
103 orbit consistency, indicated by 3D 24-h overlapping orbit differences (OODs), was found to be
104 approximately 36 cm and 88 cm for IGSO and MEO satellites respectively. SLR validation with
105 fewer normal points (NPs) from the International Laser Ranging Service (ILRS) (Pearlman et al.
106 2002) shows the radial orbit accuracy is approximately 11 cm and 40 cm for IGSO and MEO
107 satellites respectively. Similar precision is also confirmed by the 24-h OODs in radial.
108 Unfortunately, factors affecting orbit and clock quality have not been investigated and analyzed,
109 such as the yaw attitude, SRP, and onboard atomic clock performance. Recently, Zhang et al.
110 (2017) assessed the performance the BeiDou-3e satellites, and the analysis indicates that the
111 quality of the new-generation BeiDou-3 signals is comparable to that of GPS and Galileo signals.
112 In this study, we present the performance of the BeiDou-3e orbit and clock as determined by long-
113 period data, and also analyze the above-mentioned factors and their impacts. In particular, we
114 highlight the differences between BeiDou-2 and BeiDou-3e satellites in orbit, clock, and yaw
115 attitude.

116 Following the section on the overview of data collection and availability, the POD strategy is
117 described. Afterwards, the orbit boundary discontinuity (OBD) and SLR are used as the metrics to
118 evaluate the orbit quality, while the impacts of the length of POD arc, as well as number of ECOM
119 parameters on the orbits, will be investigated in order to obtain the best solution. And then, the
120 yaw attitudes are estimated and analyzed with a comparison to BeiDou-2. After assessment of the

121 stability of onboard atomic clock with modified Allan deviations (MADEVs), this study is
122 concluded in the final section.

123

124 **Data collection and availability**

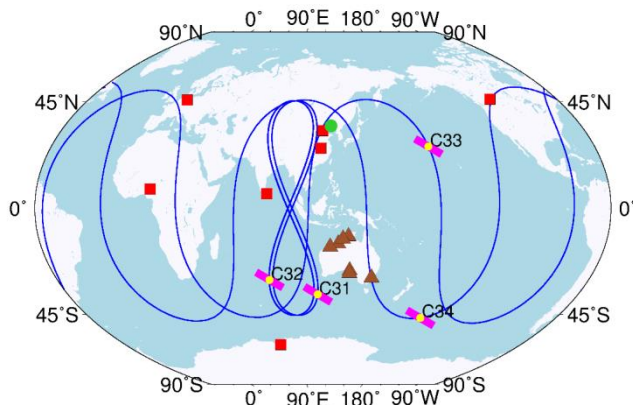
125 Signals are transmitted by BeiDou-3e satellites on as many as 5 frequencies, listed in Table 2,
126 including the backward-compatible BeiDou-2 B1I and B3I signals. The signal bandwidth,
127 modulation rate, and the signal modulation code structure can be founded in CSNO (2017). In this
128 case, BeiDou-3e satellites can be easily tracked by BeiDou-2 receivers with minor modifications.
129 In this study, 15 stations from iGMAS, BeiDou Experimental Tracking Network (BETN), and
130 Geoscience Australia (GA) network were used. Figure 1 shows their distribution. Most of the sites
131 are in the Asia-Pacific region, and this distribution results in relatively poor tracking conditions
132 for MEO satellites. Table 3 summarizes the information on the location, receiver, and antenna of
133 the 15 stations. For iGMAS stations, two kinds of receivers, CETC-54 GMR-4011 and GNSS-
134 GGR, are used. Those are manufactured by the 20th and 54th Institute
135 of China Electronics Technology Corporation respectively. The Ture-CORS receiver from Wuhan
136 Navigation and LBS Inc. and the PolRx5 receiver from Septentrio are deployed in BETN and GA
137 networks. However, all the receivers could track only the B1I and B3I signals transmitted by the
138 BeiDou-3e satellites.

139

140 **Table 2** Frequency of BeiDou-3e satellite-transmitted signals

Frequency					
Band	B1I	B3I	B1C	B2a	B2b
Frequency (MHz)	1561.098	1268.52	1575.42	1176.45	1207.14

141



142

143 **Fig. 1** Distribution of the 15 stations used and ground tracks of the BeiDou-3e satellites. Red
 144 squares indicate iGMAS, the green circle represents the BETN, and the brown triangles are GA
 145 stations

146

147 **Table 3** Information of the 15 stations used in this study

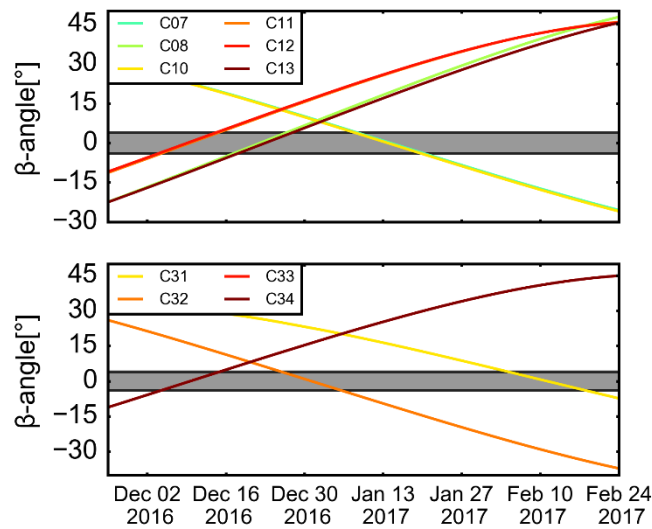
Site Abbrev.	Location	Country	Receiver code	Antenna code
CEDU	Ceduna	Australia	SEPT POLARX5	AOAD/M_T NONE
STR1	Stromlo	Australia	SEPT POLARX5	ASH701945C_M NONE
KAT1	Katherine	Australia	SEPT POLARX5	LEIAR25.R3 LEIT
THEV	Thevenard	Australia	SEPT POLARX5	LEIAR25.R3 LEIT

WLAL	Wallal	Australia	SEPT POLARX5	LEIAR25.R3 LEIT
FROY	Fitzroy Crossing	Australia	SEPT POLARX5	LEIAR25.R3 LEIT
KUNU	Kununurra	Australia	SEPT POLARX5	JAV_RINGANT_D M SCIS
ABJA	Abuja	Nigeria	GNSS_GGR	RINT-8CH CETD
BJF1	Beijing	China	CETC-54GMR- 4011	LEIAR25.R4 LEIT
BRCH	Braunschweig	Germany	CETC-54GMR- 4011	LEIAR25.R4 LEIT
CLGY	Calgary	Canada	CETC-54GMR- 4011	LEIAR25.R4 LEIT
KNDY	Kandy	Sri Lanka	CETC-54GMR- 4011	GNSS-750 NONE
WUH1	Wuhan	China	CETC-54GMR- 4011	LEIAR25.R4 LEIT
ZHON	Zhongshan Station	Antarctica	GNSS_GGR	LEIAR25.R4 LEIT
LIN6	Liaoning	China	Ture-CORS	LEIAR25.R4 LEIT

148 **Precision orbit determination strategy**

149 Three-month data from November 25, 2016 to February 25, 2017 collected by the aforementioned
150 stations are used for precise orbit and clock determination in this study. However, due to the
151 unstable performance of receivers, up to 5 stations have no data for several days, which affects the
152 orbit and clock quality. During the selected period, 10 BeiDou satellites experience the eclipse
153 period. Figure 2 shows the variations of the angle of the sun above the orbit plane (β angle) for
154 BeiDou-2 IGSO and MEO satellites (top) as well as BeiDou-3e satellites (bottom), in which the
155 gray bar indicates the region with a β angle between -4° and $+4^\circ$, when the BeiDou-2 IGSO and
156 MEO satellites switch to the ON orientation. Among those satellites, C11, C12, C33, and C34 are
157 in the same orbit plane.

158



159

160 **Fig. 2** Variations of the angle of the sun above the orbit plane (β angle) for BeiDou-2 IGSO and
161 MEO satellites (top) as well as BeiDou-3e satellites (bottom). The gray bar indicates the region
162 with a β angle between -4° and $+4^\circ$, when the BeiDou-2 IGSO and MEO satellites switch to the
163 ON orientation

164

165 To objectively compare BeiDou-2 and BeiDou-3e satellites, we determine again the orbits and
166 clocks of BeiDou-2 with BeiDou-3e simultaneously using the 15 tracking stations. All data are
167 processed by Position And Navigation Data Analyst (PANDA) software (Liu and Ge 2003) using
168 a 2-step approach. In the first step, the WUM orbits, clocks, and earth orientation parameters from
169 the IGS MGEX (Guo et al. 2015) are used for GPS/BeiDou-2 combined precise point positioning
170 (PPP) to estimate the station coordinates, tropospheric zenith delays, and receiver clock offsets.
171 The analysis by Guo et al (2017b) demonstrates that WUM Multi-GNSS products have the same
172 quality as those from other IGS MGEX ACs, e.g., CODE, and GFZ. Also, SLR validation further
173 indicates that the radial orbit accuracy for BeiDou MEO, IGSO, and GEO satellites is
174 approximately 5 cm, 10 cm, and 50 cm respectively (Guo et al. 2017b). With this product, the
175 obtained station coordinates repeatability reach to about 1cm in 3D. The estimated parameters
176 from the first step are kept fixed in the second step. We use GPS/BeiDou-2 combined PPP instead
177 of GPS only because of the poor quality of GPS data from some iGMAS stations. In the second
178 step, the ionospheric-free combination of B1I and B3I observations are taken as input with initial
179 orbits and clocks from broadcast ephemeris, because only the two backward-compatible signals
180 can be tracked, as mentioned earlier. We apply a 10° cutoff elevation and elevation-dependent
181 weighting for the observations under 30° . The satellite orbital parameters, satellite clock offsets,
182 ambiguities, and inter system bias (ISB) are estimated. For the SRP model, a 5-parameter or 9-
183 parameter ECOM model with a POD arc length from 2 to 5 d are applied to explore the effects of
184 the SRP model and the POD arc length on orbit quality. In addition, an empirical constant
185 acceleration parameter in the along-track direction with 1.0^{-10} m/s^2 constraint is estimated for each
186 satellite, as done by Guo et al. (2015). The BeiDou-3e satellite geometry and orientation follow
187 the conventions in Montenbruck et al. (2015) without considering yaw maneuvers, whereas the
188 attitude model described in Guo et al. (2017a) is used for the BeiDou-2 satellites. The measurement
189 and orbit dynamic models are summarized in Table 4, and Table 5 lists the BeiDou-3e phase center
190 offset (PCO) values provided by the satellite manufacturers.

Table 4 Summary of precise orbit determination strategy

Observable	Undifferenced ionospheric-free code and phase combination of B1 and B3
Elevation angle cutoff	10°
Sampling rate	30 s
POD arc length	2, 3, 4, and 5 d
Weight	Elevation-dependent weighting for the observations under 30° according to $1/2 \sin(E)$
Initial standard deviations	2.0 m and 2.0 cm for raw code and phase
Phase center offset	BeiDou-2: estimated values (Guo 2014) BeiDou-3e: manufacturer values in Table 5
Satellite attitude model	Nominal YS model for BeiDou-3e satellites (Montenbruck et al. 2015) ON and YS for BeiDou-2 satellites (Guo et al. 2017a)
ISB	Estimated as arc-dependent constants for each receiver
Troposphere correction	Saastamoinen model for a priori dry and wet zenith delay model with estimation of wet delay

	global mapping function for dry and wet zenith delays
Tide correction	Solid earth tides, solid earth pole tides, and ocean tides as International Earth Rotation and Reference Systems Service (IERS) conventions, 2010
Geopotential	EGM2008 with 12 degrees and orders
SRP model	5-parameter or 9-parameter ECOM
Relativistic effects	IERS conventions 2010

193

194

Table 5. Manufacturer PCO values for BeiDou-3e satellites (unit: mm)

	X	Y	Z
C31	-50	0	800
C32	-110	-300	2,000
C33	-190	0	1,500
C34	-200	0	1,400

195

196 **Orbit validation and analysis**

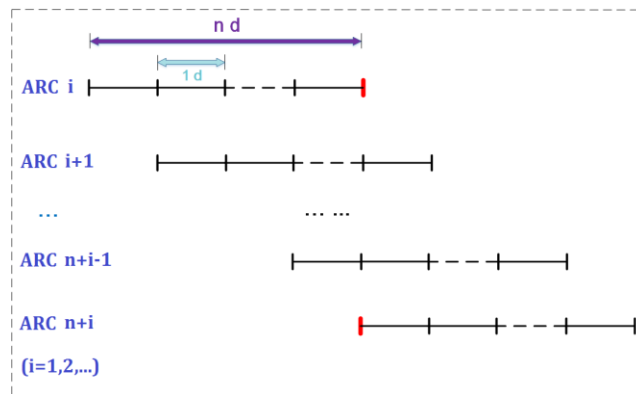
197 To investigate the impacts of the POD arc length and the number of ECOM parameters on BeiDou-
 198 3e orbit quality, eight solutions are determined and validated by OBD and SLR. In this section, we
 199 also compared the BeiDou-2 and BeiDou-3e orbits based on the validation metrics.

200

201 Orbit boundary discontinuity

202 As an internal validation of orbit quality, OBD has been proposed by Griffiths and Ray (2009)
203 using 3D position differences at a specific epoch to assess the orbit accuracy. Intrinsically, this
204 approach is similar as OODs to validate the consistency of consecutive orbits from the same AC,
205 but it does not give overly optimistic results since only one orbit at a specific epoch is used for
206 comparison. In this study, the two POD arcs with only one common midnight epoch were selected.
207 And the OBD was calculated by 3D position differences between the orbit at the last epoch of one
208 arc and the orbit at the first epoch of another arc, as shown in Figure 3.

209



210

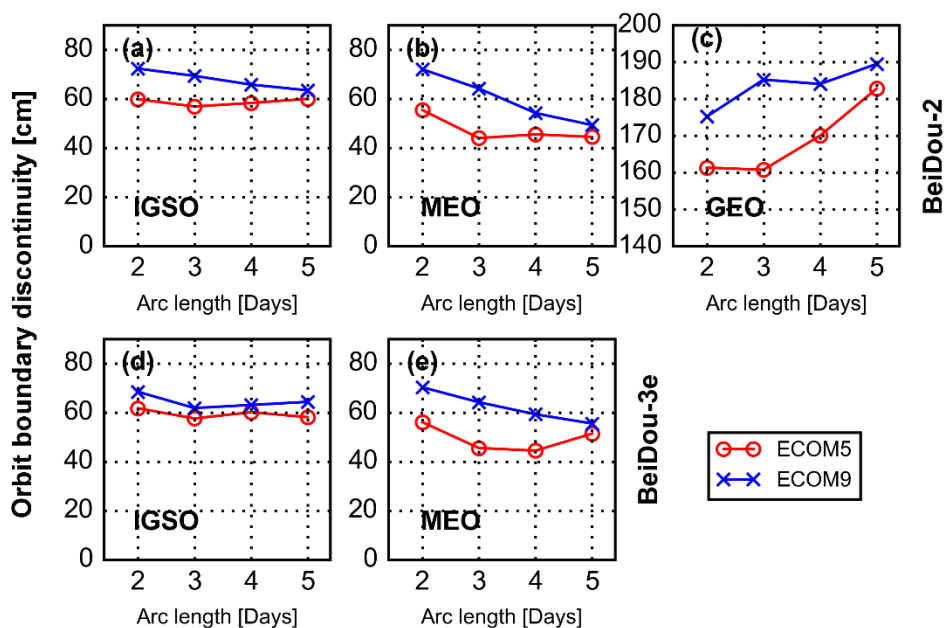
211 **Fig. 3** Orbit arcs and orbit boundary discontinuity (OBD, red vertical bar). Two POD arcs
212 (ARC i and ARC $n+i$) with only one common midnight epoch were selected. OBD is calculated
213 by 3D position differences between the orbit at the last epoch of one arc (ARC i) and the orbit at
214 the first epoch of another arc (ARC $n+i$).

215

216 Figure 4 shows the average 3D root mean square (RMS) values of each solution's OBDs for the
217 respective group, classified according to the satellite generation and types. Because the BeiDou-2
218 IGSO and MEO satellites suffer a marked degeneration of orbit quality in the ON mode, the arcs
219 containing the ON mode are excluded in the statistic for analysis. No GEO is available for BeiDou-
220 3e satellites, so the comparison is focused on IGSO and MEO satellites in the following discussion.

221 In general, the average RMS of 5-parameter ECOM (ECOM5) solutions is lower than that of 9-
 222 parameter ECOM (ECOM9) solutions with the same POD arc length. For the ECOM5 model, the
 223 smallest RMS values are obtained for solutions with a 3-day arc length. However, for ECOM9
 224 solutions the RMS values almost decrease with increasing POD arc length and reach the minimum
 225 when the POD arc length is 5 days, except for BeiDou-3e IGSO satellites, which has increasing
 226 OBD values for 4-day and 5-day arcs. This indicates that the full set of ECOM model probably
 227 require a greater POD arc length to smooth the orbit dynamics compared to reduced 5 parameters.
 228 In addition, it can be observed that the IGSO satellites show a larger average RMS than that of
 229 MEO satellites for both BeiDou-2 and BeiDou-3e, although the IGSO satellites have better
 230 tracking condition because of the Asia-Pacific regional station used in this study. This can be
 231 attributed to the larger nadir angle caused by the lower orbit altitude of MEO satellites, which
 232 makes the orbit dynamic parameters easier to separate from the other estimated parameters. In
 233 addition, the long POD arc may also have helped to smooth the orbit dynamic parameters of the
 234 MEO satellites and reduce the deficiency of the data coverage. In general, the best orbits for
 235 BeiDou satellites can be determined with the ECOM5 model and a 3-day POD arc.

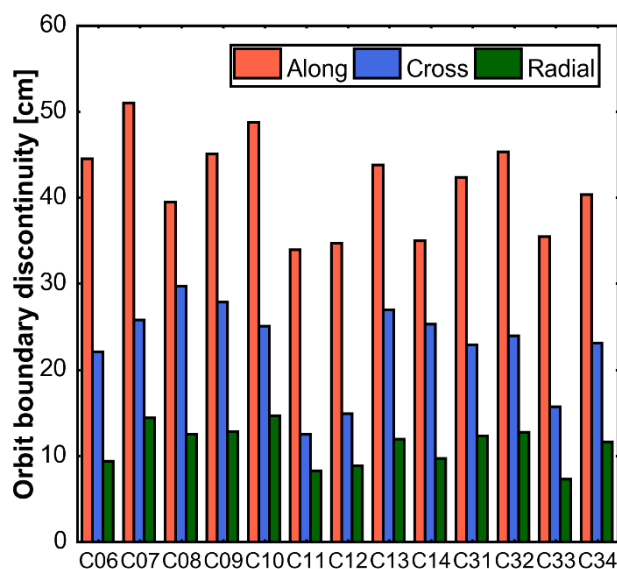
236



237

238 **Fig. 4** Average 3D RMS values for OBDs for the respective groups classified according to the
 239 satellite generation and types. (a) BeiDou-2 IGSO, (b) BeiDou-2 MEO, (c) BeiDou-2 GEO, (d)
 240 BeiDou-3e IGSO, and (e) BeiDou-3e MEO. Five-parameter (ECOM5) and 9-parameter
 241 (ECOM9) ECOM solutions are indicated as red circles and blue crosses respectively

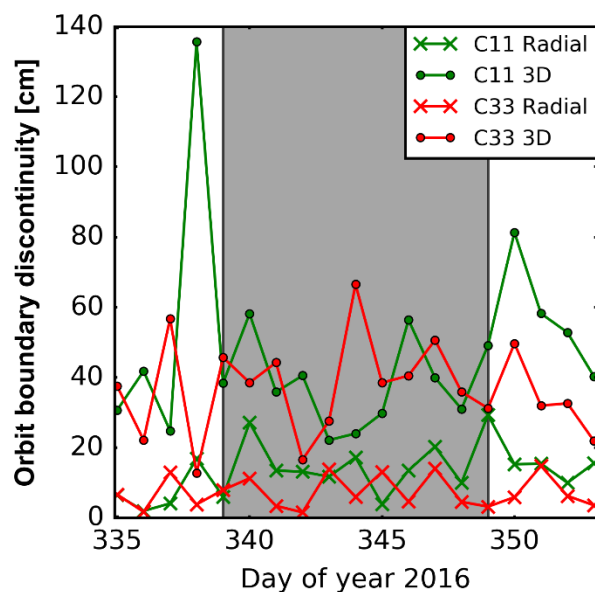
242
 243 Furthermore, Figure 5 shows the average RMS values of OBDs for the best solutions, i.e.,
 244 using the ECOM5 model with 3d data arcs, in along-track, cross-track, and radial directions. In
 245 general, the orbit consistency is approximately 30 to 50 cm, 10 to 30 cm, and 8 to 15 cm in along-
 246 track, cross-track, and radial directions respectively. Similar performance is achieved for BeiDou-2
 247 and BeiDou-3e satellites.



248
 249 **Fig. 5** Average RMS values of BeiDou-2 and BeiDou-3e OBDs for the solution determined
 250 with the ECOM5 model and a 3-d arc in along-track, cross-track, and radial directions

251
 252 As mentioned earlier, the 4 MEO satellites (C11, C12, C33, and C34) are in the same orbit
 253 plane, however, different performances are observed for C33/C34 and C11/C12 as shown in Figure

254 5, particularly in the along-track direction. Studying the daily RMS of OBDs, marked performance
 255 differences are identified when the β angle is between -4° and $+4^\circ$. Figure 6 shows the daily 3D
 256 and radial RMS for the best solution of C11 and C33 during DOY 339 to 349, 2016. It is clear that
 257 the orbit accuracy degenerates significantly after C11 switches its attitude mode, whereas C33
 258 shows stable orbit performance. This indicates the different yaw attitude control mode used by
 259 BeiDou-3e satellites when the β angle is between -4° and $+4^\circ$.



260
 261 **Fig. 6** Daily 3D and radial RMSs of OBDs for C11 and C33 during DOY 339 to 349, 2016,
 262 when C11 switches its attitude mode to ON mode indicated by grey block region.

263
 264 Satellite laser ranging validation
 265 SLR is used for independent validation of GNSS satellites' orbits mainly in the radial component.
 266 All launched BeiDou-3e satellites are equipped with laser retroreflectors (LRAs) and are tracked
 267 by the ILRS. The LRA coordinates in the satellite reference frame of BeiDou-3e satellites are listed
 268 in Table 6. In this study, only the first 24 h orbits in each solution are used for SLR validation.
 269 Table 7 summarizes the results. Residuals larger than 2.0 m, 1.0 m, and 1.0 m for GEO, IGSO,

270 and MEO satellites, respectively, are treated as outliers and removed. After quality control, there
 271 are 845, 872, 714, 1130, 115, 120, and 119 NPs left for C01, C08, C10, C11, C32, C33, and C34
 272 respectively. Unfortunately, no NPs are available for C31 during the study period. In contrast to
 273 BeiDou-2 satellites, there are fewer NPs for BeiDou-3e satellites, because the SLR tracking
 274 priority is quite low.

275

276 **Table 6** LRA offsets for BeiDou-3e satellites (unit: m)

	X	Y	Z
C31	-0.973	0.184	0.637
C32	0.185	0.685	1.960
C33	0.612	-0.072	1.249
C34	0.612	-0.072	1.245

277

278 **Table 7** RMS of SLR residuals for different BeiDou-2 and BeiDou-3e orbit solutions (unit:
 279 cm)

Arc length								
	(days)	C01	C08	C10	C11	C32	C33	C34
	2	30.1	17.9	19.2	16.0	18.9	10.1	12.9
ECO	3	31.6	17.2	18.9	14.3	17.1	9.8	10.5
M5	4	32.0	20.9	19.2	14.5	17.3	8.7	12.1
	5	32.6	23.1	19.7	14.5	18.7	10.2	12.0

	2	33.8	32.8	32.9	43.0	44.3	14.4	18.7
ECO	3	31.3	31.1	25.5	17.2	41.9	13.3	18.0
M9	4	31.7	29.2	23.2	15.0	29.7	11.1	14.2
	5	30.8	28.8	22.1	14.7	22.7	12.5	13.9

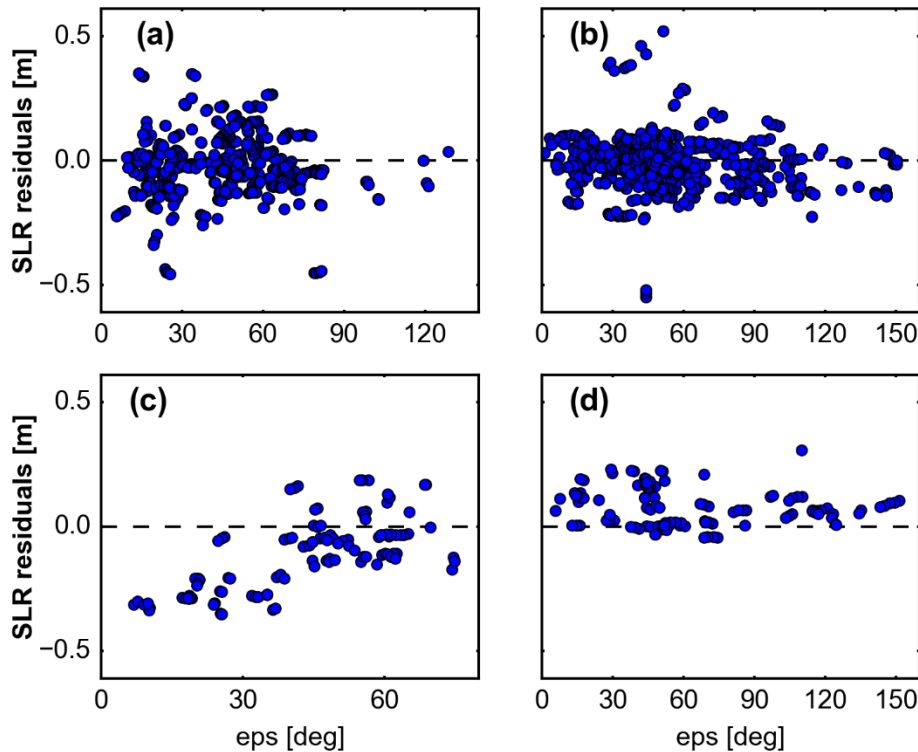
280

281 In general, from the SLR validation the same conclusion can be drawn as for OBDs: The
 282 ECOM5 solutions are superior to ECOM9 solutions with the same POD arc length, regardless of
 283 the type or generation of the BeiDou satellite. MEO satellites show better performance than that
 284 of IGSO satellites. As to the POD arc length, 3-day is the best for the ECOM5 model and 5-day
 285 for the ECOM9 model. Among all the solutions, the orbits determined with the ECOM5 model
 286 and a 3-day arc have the best performance. Similar orbit precision has been achieved for BeiDou-
 287 2 and BeiDou-3e IGSO satellites, whereas the BeiDou-3e MEO orbits show better performance
 288 than that of IGSOs as validation by OODs. The RMS value of SLR residuals for the best solution
 289 of BeiDou-3e C33 and C34 reaches to approximately 10 cm, although the eclipse season is also
 290 included.

291 To illustrate the results of our investigation into whether systematic error is induced by the
 292 deficiency of the SRP model in BeiDou-3e satellites, Figure 7 shows the SLR residuals of the best
 293 solution against the sun elongation angle (eps angle, the angle formed by earth–spacecraft–sun)
 294 for 2 IGSO (C08 and C32) and 2 MEO (C11 and C33) satellites. Although fewer NPs are available
 295 for C33, it can be seen that there is no systematic error in the SLR residuals, except a minor positive
 296 bias, this may be caused by the inaccuracy of LRA offsets listed in Table 5. Almost no any
 297 systematic error exists for C11. For the 2 IGSO satellites, a different pattern of SLR residuals can
 298 be observed. For C32, there is an obvious linear increasing trend in the SLR residuals that is not
 299 found for C10. This indicates that there are sun-elongation-angle-dependent systematic errors in
 300 C32 orbits, and reflects the deficiency of the ECOM SRP model for C32 POD. Similar errors have

301 been identified for Galileo satellites (Montenbruck et al. 2015), hence an enhanced SRP model for
302 C32 is required for further research.

303



304

305 **Fig. 7** SLR residuals against the Sun elongation angle (eps angle) for (a) C08, (b) C11, (c) C32,
306 and (d) C33

307

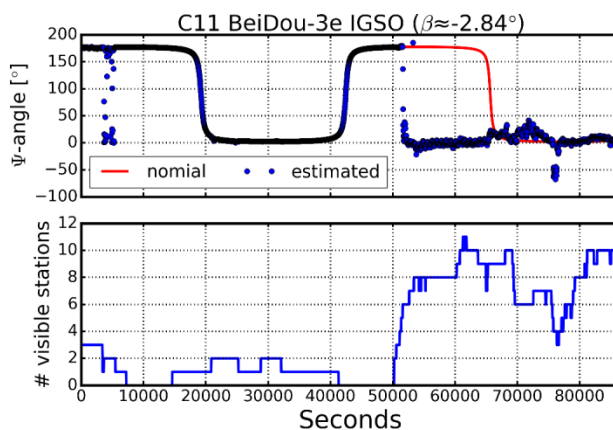
308 **Yaw attitude estimation**

309 As shown above, different performances are shown by BeiDou-2 and BeiDou-3e satellites when
310 the β angle is between -4° and $+4^\circ$. In that case, the BeiDou-2 IGSO and MEO satellites switch to
311 the ON orientation when yaw angles (Ψ defined by the angle between the instantaneous velocity
312 and the body-fixed x-axis) are set to zero. We infer from this that different attitude control mode
313 is adopted by BeiDou-2 and BeiDou-3e satellites. To validate this, we estimate the yaw attitude of
314 BeiDou-3e IGSO and MEO satellites based on the reversed kinematic PPP approach (Dillsner

315 et al. 2011). The parameters obtained from the POD steps, i.e., the station coordinates, receiver
316 clock offset, ZTD values, orbits, and ISB and ambiguities, are fixed in the yaw attitude estimation.
317 In that case, only the epoch-wise satellite PCO values and clock offsets are estimated as white
318 noise. Concerning the few decimeters of orbit accuracy achieved, the yaw attitude cannot be
319 estimated accurately for C31, because the PCO offset in X-axis is only 5 cm for C31.

320 Also, one may question whether it is possible to estimate the yaw attitude correctly from only
321 15 stations. Hence, we have estimated the C11 yaw profile to check that possibility and the
322 accuracy achieved. Figure 8 demonstrates the estimated yaw profile and the number of stations
323 used for estimation on DOY 341, 2016, when the satellite is in the ON mode with an approximately
324 -2.84° β angle. In this case, the real yaw angles are 0° . However, because less than 2 stations are
325 available for attitude estimation from the Asia-Pacific region (0 to 50,000 s), the estimated yaw
326 angles equal to the nominal model angle instead of 0° . Once the satellite is above the Asia-Pacific
327 region, starting at 50,000 s, more than 5 stations track the satellite and could be used for attitude
328 estimation. In this case, the estimated yaw angles approach 0° with better than 10° accuracy. When
329 there are more than 7 stations, a more stable yaw estimation is obtained. The result confirms that
330 it is possible to estimate the yaw angle within approximately 10° even with a limited number of
331 stations.

332

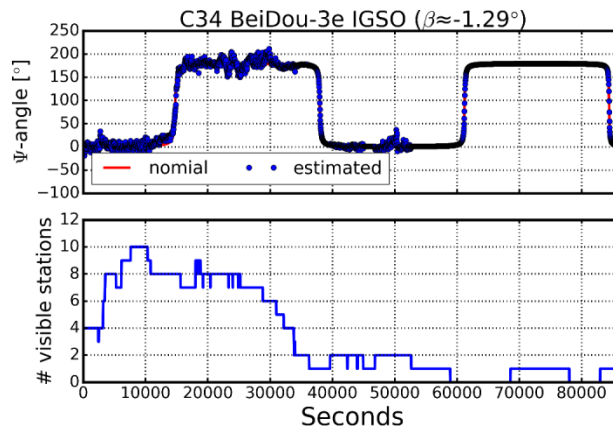


333

334 **Fig. 8** C11 estimated yaw profile and the number of stations used on DOY 341, 2016 (-2.84° β
335 angle). The red line in the top panel represents the nominal yaw angle, and the blue dots indicate
336 the epoch-wise estimated yaw angle. The bottom panel indicates the number of stations used for
337 attitude estimation in each epoch.

338 Figures 9 and 10 show the estimated yaw attitude profiles for C34 (MEO) and C32 (IGSO)
339 when they are in deep eclipse season (-1.29° and 0.57° β angle for C34 and C32). In contrast with
340 C11, the estimated yaw angles are almost identical to their nominal attitude and do not approach
341 0° . Similar phenomena are found for C33. For C32, the estimated yaw profile still obeys the
342 nominal GNSS attitude. Hence, BeiDou-3e satellites do not use the ON mode in the eclipse season
343 as BeiDou-2 IGSO and MEO satellites do.

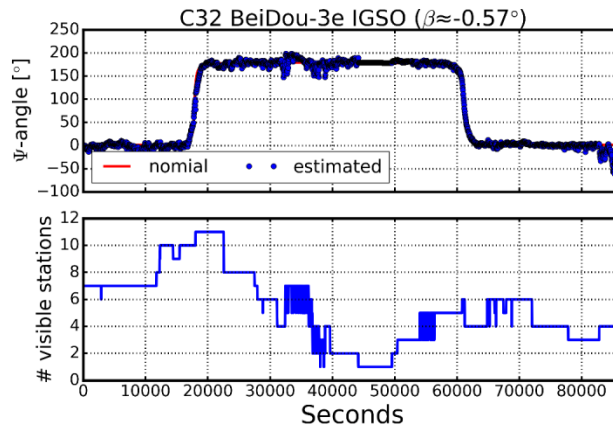
344



345

346 **Fig. 9** C34 estimated yaw profile and the number of stations used on DOY 343, 2016 (-1.29° β
347 angle). In the top panel, the red line represents nominal yaw angle, and the blue dots indicate the
348 epoch-wise estimated yaw angle. The bottom panel indicates the number of stations used for
349 attitude estimation in each epoch.

350

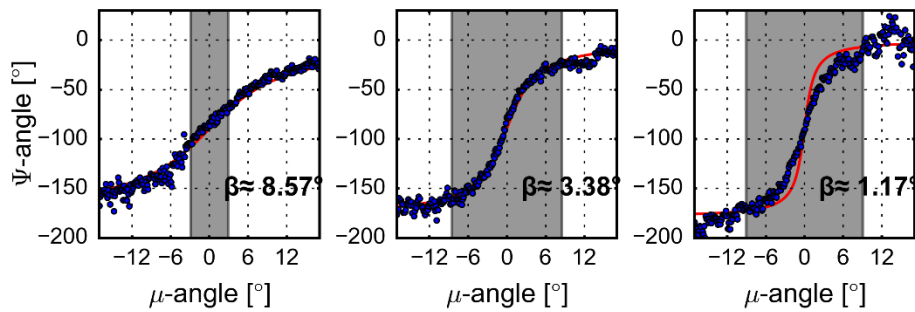


351
 352 **Fig. 10** C32 estimated yaw profile and the number of stations used on DOY 1, 2017 (-0.57° β
 353 angle). In the top panel, the red line represents nominal yaw angle, and the blue dots indicate the
 354 epoch-wise estimated yaw angle. The bottom panel indicates the number of stations used for
 355 attitude estimation in each epoch.

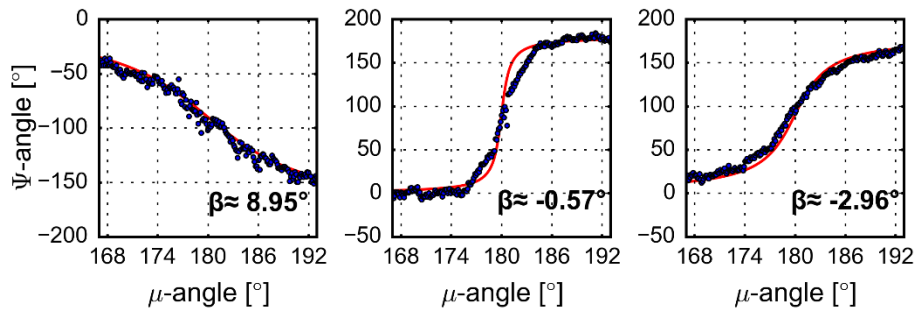
356
 357 It could be argued that the inaccurate PCO values on the x- and y-axes contaminate the
 358 estimation of yaw attitudes. However, for the satellites with the mean antenna phase center located
 359 within the XZ plane, such as C31, C33, and C34, the X PCO values do not affect the yaw attitude
 360 estimation, as it is canceled when the yaw bias is estimated. For those with an antenna offset in the
 361 y-axis, the inaccurate X and Y PCOs actually result a yaw rotation with the angle between the
 362 inaccurate PCO vector and the true one in the XY plane. In this case, the angle will contaminate
 363 the estimation and show as a constant bias in the estimated yaw attitudes. However, the precision
 364 of the C32 X and Y PCO values listed in Table 4 is within 10 cm, which results in less than 1°
 365 angle biases. Considering that the yaw estimation accuracy is approximately 10° , the effect of
 366 inaccurate X and Y PCOs can be ignored.

367 To study the attitude control mechanism of BeiDou-3e IGSO and MEO satellites, we further
 368 investigate the estimated yaw attitudes. No eclipse-crossing maneuvers are identified, but
 369 maneuvers near the midnight point (orbit angle $\mu=0^\circ$) and noon point ($\mu=180^\circ$) are observed.
 370 Figures 11 and 12 show the yaw profiles during eclipse phases for C32 near the midnight and noon

371 points respectively. It can be seen that both yaw attitude maneuvers show similar variations and
 372 patterns. The yaw attitudes are symmetric to the midnight or noon point and match the nominal
 373 attitude when the satellite is in the midnight or noon point. The yaw attitudes near the midnight
 374 and noon points are also investigated for the two MEO satellites C33 and C34, where similar
 375 variations are identified. With careful analysis of the yaw profiles, we find that the yaw attitude
 376 maneuvers occur when the β angle is between -3° and 3° . Considering the 10° accuracy for the
 377 estimated yaw attitude, we do not intend to establish the attitude model but leave it for further
 378 study when more tracking stations and accurate yaw estimates will be available.



379
 380 **Fig. 11** Estimated (blue) and nominal (red) yaw angles of BeiDou-3e C32 passing the Earth's
 381 shadow (gray area) under different β angles



383
 384 **Fig. 12** Estimated (blue) and nominal (red) yaw angles of BeiDou-3e C32 passing the region
 385 around orbit noon under different β angles

386

387 **Clock performance**

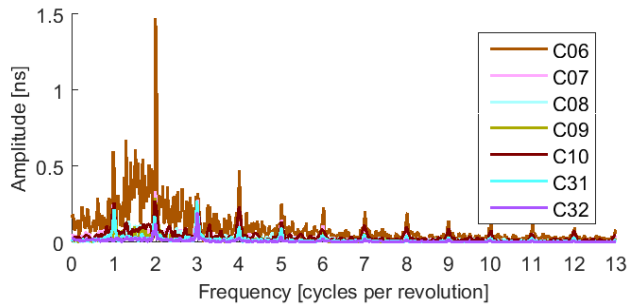
388 The stability of onboard satellite clocks will affect the accuracy of the predicted clock offsets, as
389 well as the performance of the PNT service. Therefore, highly stability atomic clocks are required.
390 Unlike the BeiDou-2 satellites, which are equipped with rubidium clocks from manufacturers in
391 Switzerland and China, the primary frequency standards of BeiDou-3e satellites are based on
392 PHMs, and the improved Chinese RAFSs serve as the backup.

393 Power spectrum analysis of Beidou satellite clocks

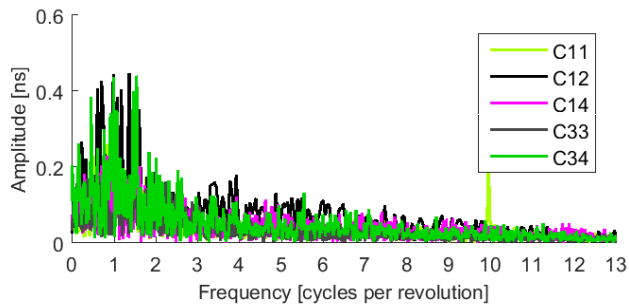
394 Since the satellite clocks are highly correlated with the orbits, particularly in the radial, the orbit
395 errors will be leaked to clock offsets. Hence, there may be some orbit mis-modeling errors in the
396 apparent clock variations. In order to quantify the correlation between the orbit and clocks, a power
397 spectrum analysis of satellite clocks has been performed. The Fourier transform method is used to
398 identify the potential periodicity of satellite clocks. Non-equispaced or non-uniform fast Fourier
399 transforms (NUFFT) are used in this study to avoid the impact of data gaps on the analysis result.
400 Since the biggest influences caused by the relativistic J_2 contribution (Kouba 2014) is 33 ps and
401 67 ps for IGSO and MEO satellites respectively, the systematic variation is not corrected. The
402 detrended daily data are stacked for NUFFT.

403 Figure 13 shows the amplitude spectrum of IGSO (top) and MEO (bottom) satellite clocks.
404 For BeiDou-2 and BeiDou-3e IGSO satellites, the 12 h (two cycles per revolution or cpr) and 24
405 h (1 cpr) harmonics are significant, particularly for C06 satellites. There are noticeable signals in
406 8 h (3 cpr) and 6 h (4 cpr). Then, with increasing number of cpr, the amplitudes decrease gradually.
407 Similar results have been identified in Wang et al (2016). However, a broad spectrum within 2 cpr
408 is observed for MEO satellites, making it hard to identify the periodicity of satellite clocks.
409 Compared with those obtained in Wang et al (2016), which shows clear periodic signals in BeiDou-
410 2 MEO satellite clocks, this may be caused by the limitation of regional stations used to track the
411 MEO satellites as well as relative short period used for analysis.

412



413



414

415 **Fig. 13** Amplitude spectrum of BeDou-2 and BeiDou-3e IGSO (top) and MEO (bottom) satellite
416 clocks

417

418 These periodic cpr signals of satellite clocks can be caused by the orbit errors. Hence, in order
419 to make reliable assessment of the background stability of BeiDou onboard frequency standards,
420 the following model is used to fit the periodic signals at 1-, 2-, 3, and 4-cpr of satellite clocks, as
421 those amplitudes are most pronounced as shown in Figure 13,

422

$$f(t) = (a + b \cdot t) + \sum_{i=1}^4 [c_i \cdot \cos(i\mu) + s_i \cdot \sin(i\mu)] \quad (1)$$

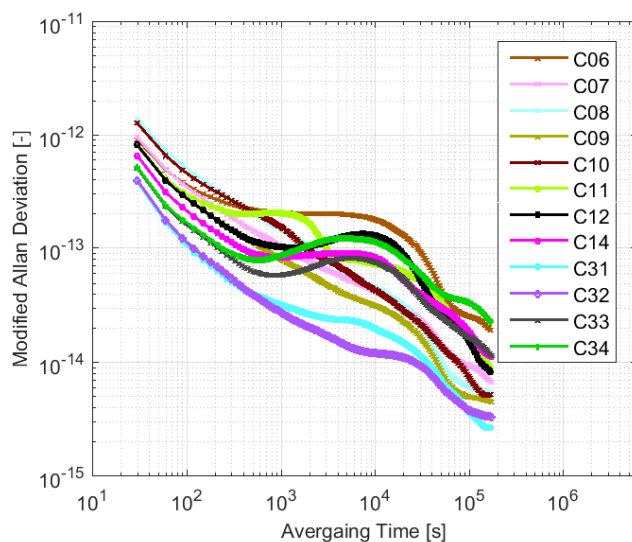
423 where a , b , c_i , and s_i are the parameters to be fitted, $f(x)$ is the fitted signals in clocks. The
424 obtained sub-daily signals will be removed from clock offsets.

425

426 Frequency stability analysis of Beidou satellite clocks

427 To assess the performance of the BeiDou onboard clocks, MADEVs computed from the 30 s clock
428 estimates are shown in Figure 14. Before the computation, the outliers, clock jumps, frequency
429 steps and also the sub-daily periodics in the satellite clock offsets obtained above are carefully
430 investigated and removed. In general, the BeiDou onboard clocks are affected by phase flicker
431 noises in the short period (30 s to 60 s) and by frequency white noise in the medium period (60 s
432 to 2,000 s). For an integration time beyond 2,000 s, both of BeiDou-2 and BeiDou-3e MEO
433 satellites display complex, non-power-law behavior, and a “bump” appears at approximately
434 10,000 s. These may be attributed to the broad spectrum within 2 cpr signals in the clock offsets
435 shown in the Fig. 3. Considering there are no such behaviors for BeiDou-2 MEO satellites in Wang
436 et al (2016), the variations are unconvinced. Hence, in this study, only the MADEVs of IGSO
437 satellites are used to assess the BeiDou-3e onboard clock performance.

438



439

440 **Fig. 14** Frequency stability analysis result after removing the sub-daily periodics

441

442 For BeiDou-2 IGSO satellites, at an integration time of 1,000 s, the MADEV values for all
443 satellites are approximately $1-3 \times 10^{-13}$ and vary approximately as $3 \times 10^{-12} \cdot (\tau/s)^{-1/2}$. Similar results
444 are shown in Montenbruck et al. (2017). However, we find a slightly worse performance in this
445 study, because fewer stations are used for satellite clock determination. For BeiDou-3e IGSO
446 satellites, the frequency stability of onboard clocks is better than that of the BeiDou-2, the MADEV
447 value is approximately $2-4 \times 10^{-14}$ at an integration time of 1,000 s, which is better than that of
448 BeiDou-2 IGSO satellites by almost a factor of 10. These results confirm that better RAFSs and
449 PHMs are used by BeiDou-3e satellites. In addition, compared to the latest type of RAFSs
450 employed onboard the GPS IIF satellites, as well as the PHMs used onboard the Galileo satellites,
451 which exhibit stabilities of $1-2 \times 10^{-12} \cdot (\tau/s)^{-1/2}$ (Montenbruck et al. 2017), similar performance is
452 achieved for BeiDou-3e onboard frequency standards, as shown by C31 and C32.

453

454 **Summary and discussion**

455 In this study, 3 months of data from GA, iGMAS, and BETN are used for orbit and clock
456 determination of BeiDou-2 and BeiDou-3e satellites based on the ECOM SRP model. For
457 comparison, eight solutions are determined with different numbers of ECOM SRP parameters as
458 well as POD arc lengths. We determine that the best solution is obtained for BeiDou-3e satellites
459 with 5-parameter ECOM and a 3-day POD arc. The 3D orbit consistency is 50 to 70 cm, and 40 to
460 60 cm for IGSO and MEO satellites, and better than 15 cm in the radial. Satellite laser ranging
461 (SLR) validation obtains to about 17 cm and 10 cm for BeiDou-3e IGSO and MEO satellites.
462 However, sun-elongation-angle-dependent orbit errors are identified in the SLR residuals of the
463 BeiDou-3e IGSO C32 satellite, which indicates the deficiency of the ECOM model for BeiDou-
464 3e IGSO satellites and requires further study.

465 Compared with the orbits of BeiDou-2 and BeiDou-3e, similar quality of orbit consistency
466 indicated by OBD is achieved, whereas BeiDou-3e show slightly better SLR validation,

467 particularly for MEO satellites. Importantly, no orbit accuracy degeneration is observed for
468 BeiDou-3e satellites when the β angle is between -4° and $+4^\circ$. In an analysis of the yaw attitude,
469 we find that BeiDou-3e satellites do not use the ON mode, but experience midnight and noon point
470 maneuvers when the β angle is approximately between -3° and $+3^\circ$. BeiDou-3e IGSO satellites
471 show better performance than that of BeiDou-2 IGSO satellites, and can be compared to the latest
472 type of RAFSSs employed onboard the GPS IIF satellites as well as the PHMs used onboard the
473 Galileo satellites with stability of $1-2 \times 10^{-12} \cdot (\tau/s)^{-1/2}$. A larger tracking network, in particular a
474 global network, is essential for further improvement of BeiDou-3 orbits, clocks, and yaw attitude
475 estimation. This will definitely change soon with the rapid development of Multi-GNSS activities.

476 **Acknowledgment**

477 The IGS MGEX, iGMAS, and ILRS are greatly acknowledged for providing the multi-GNSS
478 and SLR tracking data. The research is partially supported by the National Natural Science
479 Foundation of China (Grant No. 41504009, 41574030). Finally, the authors are also grateful for
480 the comments and remarks of two reviewers and editor, which helped to significantly improve the
481 manuscript.

482 **References**

- 483 Beutler G, Brockmann E, Gurtner W, Hugentobler U, Mervart L, Rothacher M. (1994) Extended
484 orbit modeling techniques at the CODE processing center of the International GPS Service
485 for Geodynamics (IGS): Theory and initial results. *Manuscripta Geodaetica* 19(6):367–386.
- 486 CSNO (2016) BeiDou Navigation Satellite System Signal In Space Interface Control Document
487 Open Service Signal (Version 2.1). China Satellite Navigation Office.
- 488 CSNO (2017) BeiDou Navigation Satellite System Signal In Space Interface Control Document
489 B1C and B2a Open Service Signal (Test version) (in Chinese). China Satellite Navigation
490 Office.

491 Dilssner F, Springer T, Gienger G, Dow J (2011) The GLONASS-M satellite yaw-attitude model.
492 Advances in Space Research 47(1):160-171. doi: 10.1016/j.asr.2010.09.007

493 Feng W, Guo X, Qiu H, Zhang J, Dong K (2014) A study of analytical solar radiation pressure
494 modeling for BeiDou navigation satellites based on raytracking method. In: Sun, J., Jiao, W.,
495 Wu, H., Shi, C. (Eds.), Proc. China Satellite Navigation Conference (CSNC) 2014. Vol. II.
496 Lecture Notes in Electrical Engineering 304:41-53. doi:10.1007/978-3-642-54743-0_35

497 Griffiths J, Ray J (2009) On the precision and accuracy of IGS orbits. Journal of Geodesy 83(3-4),
498 277-287. doi:10.1007/s00190-008-0237-6

499 Guo J (2014) The impacts of attitude, solar radiation and function model on precise orbit
500 determination for GNSS satellites. PhD Dissertation (in Chinese with English abstract),
501 GNSS Research Center, Wuhan University, Wuhan, China.

502 Guo J, Xu X, Zhao Q, Liu J (2015) Precise orbit determination for quad-constellation satellites at
503 Wuhan University: strategy, result validation, and comparison. Journal of Geodesy
504 90(2):143-159. doi: 10.1007/s00190-015-0862-9

505 Guo J, Chen G, Zhao Q, Liu J, Liu X (2017a) Comparison of solar radiation pressure models for
506 BDS IGSO and MEO satellites with emphasis on improving orbit quality. GPS Solutions
507 21(2):511-522, doi: 10.1007/s10291-016-0540-2

508 Guo F, Li X, Zhang X, Wang J (2017b) Assessment of precise orbit and clock products for Galileo,
509 BeiDou, and QZSS from IGS Multi-GNSS Experiment (MGEX). GPS Solutions 21(1):279-
510 290, doi: 10.1007/s10291-016-0523-3

511 Kouba J (2004) Improved relativistic transformations in GPS. GPS solutions 8(3): 170-180, doi:
512 10.1007/s10291-004-0102-x

513 Liu J, Ge M (2003) PANDA software and its preliminary result of positioning and orbit
514 determination. Wuhan University of Journal of Nature Science 8(2B):603-609.
515 doi:10.1007/BF02899825

516 Lou Y, Liu Y, Shi C, Yao X, Zheng F (2014) Precise orbit determination of beidou constellation
517 based on bets and mgex network. *Scientific Reports* 4(8):4692. doi:10.1038/srep04692

518 Montenbruck O, Steigenberger P, Hugentobler U (2014) Enhanced solar radiation pressure
519 modeling for Galileo satellites. *Journal of Geodesy* 89(3):283-297. doi:10.1007/s00190-014-
520 0774-0.

521 Montenbruck O, Schmid R, Mercier F, Steigenberger P, Noll C, Fatkulin, Kogure S, Ganeshan AS
522 (2015) GNSS Satellite Geometry and Attitude Models. *Advances in Space Research*
523 56(6):1015-1029. doi:10.1016/j.asr.2015.06.019

524 Montenbruck O, Steigenberger P, Prange L, Deng Z, Zhao Q, Perosanz F, Romero I, Noll C, Stürze
525 A, Weber G (2017) The Multi-GNSS Experiment (MGEX) of the International GNSS
526 Service (IGS) – Achievements, prospects and challenges. *Advances in Space Research*
527 59(7):1671-1697. doi:10.1016/j.asr.2017.01.011

528 Pearlman MR, Degnan JJ, Bosworth JM (2002) The International Laser Ranging Service.
529 *Advances in Space Research* 30(2):135-143. doi:10.1016/S0273- 1177(02)00277-6

530 Prange L, Orliac E, Dach R, Arnold D, Beutler G, Schaer S, Jäggi A (2016) CODE's five-system
531 orbit and clock solution—the challenges of multi-GNSS data analysis. *Journal of Geodesy*
532 91(4):345-360. doi:10.1007/s00190-016-0968-8

533 Springer TA, Beutler G, Rothacher M (1999) A new solar radiation pressure model for GPS
534 satellites. *GPS Solutions* 3(2):50–62. doi:10.1007/PL00012757

535 Steigenberger P, Hugentobler U, Hauschild A, Montenbruck O (2013) Orbit and clock analysis of
536 compass GEO and IGSO satellites. *Journal of Geodesy* 87(6):515–525. doi:10.1007/s00190-
537 013-0625-4

538 Tan B, Yuan Y, Wen M, Ning Y, Liu X (2016) Initial results of the precise orbit determination for
539 the new-generation Beidou satellites (Beidou-3) based on the iGMAS network. *ISPRS*
540 *International Journal of Geo-Information* 5(11):196. doi:10.3390/ijgi5110196

- 541 Wang B, Lou Y, Liu J, Zhao Q, Su X (2016) Analysis of BDS satellite clocks in orbit. GPS
542 Solutions 20(4): 783-794, doi:10.1007/s10291-015-0488-7
- 543 Yang D, Yang J, Li G, Zhou Y, Tang C (2017) Globalization highlight: orbit determination using
544 BeiDou inter-satellite ranging measurements. GPS Solutions. doi: 10.1007/s10291-017-
545 0626-5.
- 546 Zhang X, Wu M, Liu W, Li X, Yu S, Lu C, Wickert J (2017) Initial assessment of the
547 COMPASS/BeiDou-3: new-generation navigation signals. Journal of Geodesy. doi:
548 10.1007/s00190-017-1020-3
- 549 Zhao Q, Guo J, Li M, Qu L, Hu Z, Shi C, Liu J (2013) Initial results of precise orbit and clock
550 determination for COMPASS navigation satellite system. Journal of Geodesy 87(5):475-486.
551 doi: 10.1007/s00190-013-0622-7.

552 **Author Biographies**



553

554 Qile Zhao is a professor at GNSS Research Center of Wuhan University. He received his Ph.D.
555 degree at Wuhan University in 2004. In 2006–2007, as a postdoctoral fellow, he did his
556 postdoctoral program in DEOS, Delft University of Technology, the Netherlands. His current
557 research interests are precise orbit determination of GNSS and low earth orbiting satellites, and
558 high-precision positioning using GPS, Galileo and BDS systems.



559

560 Chen Wang is a Ph.D. student at GNSS Research Center, Wuhan University currently. He received
561 his bachelor degree at College of Geology Engineering and Geomatics, Chang'an University in
562 2014. His research focuses on GNSS data processing and precise orbit determination.



563

564 Jing Guo is a postdoctoral researcher at GNSS Research Center of Wuhan University. He received
565 his bachelor, master and doctor degrees at Wuhan University in 2009, 2011 and 2014, respectively.
566 Currently, he works on GNSS data processing, particularly the precise orbit determination for
567 multi- GNSS satellites, and is also responsible for the routine data processing of MGEX and
568 iGMAS at Wuhan University.

569



570

571 Bin Wang is currently a postdoctoral researcher at the Shanghai Astronomy Observatory, China
572 Academy of Science. He received his Master's and PhD degree from Wuhan University in 2011
573 and 2015. His current research focus is on characteristic analysis and prediction of GNSS satellite
574 clock.

575



576

577 Jingnan Liu graduated from the former Wuhan College of Surveying and Mapping in 1967 and
578 received his master's degree in 1982. He was elected Academician of the Chinese Academy of
579 Engineering in 1999. Since 1998, he has been in charge of the National Engineering Research
580 Center for Satellite Positioning System. He has been a member of the Science and Technology
581 Commit- tee, Ministry of Education of China in 1997–2009 and as an editorial board member of
582 GPS Solutions in 1998–2000. He is currently an executive member of the council, Chinese Society
583 for Geodesy, Photogrammetry and Cartography; the editorial board member of GPS World; and
584 the coordinator of IGS.